

Rocky fragments in the largest track of comet 81P/Wild 2—Chondrule debris formed in the icy outer solar system? M. Zhang¹, D. E. Brownlee², D. J. Joswiak², and N. T. Kita¹, ¹WiscSIMS, Department of Geoscience, University of Wisconsin–Madison, Madison, WI 53706, USA (mzhang467@wisc.edu), ²Department of Astronomy, University of Washington, Seattle, WA 98195, USA

Introduction: Aerogel tracks of comet 81P/Wild 2 contain abundant rocky fragments that show close affinities to primitive chondrite chondrules on petrography, Fe-Mn systematics in olivine, oxygen isotopes, and Al-Mg chronology [1-10]. Thus, they are believed to be chondritic materials that drift outward from carbonaceous and non-carbonaceous chondrite-forming regions to the comet accretion region [1-3]. Previous oxygen isotope comparison of 37 Wild 2 fragments with chondrules indicate a major source of CR chondrule-like materials and a minor source of ordinary or CH-CB chondrules [4-9]. Furthermore, the inferred sources could be more definitive if large ($\geq 5 \mu\text{m}$) Wild 2 fragments are available, which enable multiple analyses that reduce the uncertainty of $\Delta^{17}\text{O}$ to $\leq 2\text{‰}$. Here we investigated silicate fragments in track 227—the largest type B track ($\sim 17 \text{ mm}$ long) extracted from the Stardust mission. It contains abundant $\geq 2 \mu\text{m}$ (up to $20 \mu\text{m}$) fragments in the bulb region and the $60 \times 50 \mu\text{m}$ terminal particle (TP) with porphyritic texture.

Samples and methods: We have so far mined 53 fragments from T227 (including the six reported in [7]). After mineralogic examination using FE-SEM and SEM/TEM-EDS, they were measured for oxygen isotope ratios using the WiscSIMS CAMECA IMS-1280 following the procedure in [5-7]. Three primary ion beam settings were used, with $\sim 3 \mu\text{m}$ beam for olivine in the TP, $\sim 1 \mu\text{m}$ beam for an Al-diopside, and $\sim 2 \mu\text{m}$ beam for the majority, giving an uncertainty for $\Delta^{17}\text{O}$ of $\sim 1\text{‰}$, $\sim 6\text{‰}$, and $\sim 2\text{‰}$, respectively. Thirty-four fragments with sizes $\geq 5 \mu\text{m}$ were analyzed 2-6 times using the $2 \mu\text{m}$ beam. The result nearly tripled the oxygen isotope dataset of Wild 2 fragments.

Results: The 53 Wild 2 fragments display diverse mineralogy (13 chondrule-like) and wide ranges of chemistry (Mg#: 100 to 52) and oxygen isotope ratios ($\Delta^{17}\text{O}$: $\sim -22\text{‰}$ to $\sim 7\text{‰}$).

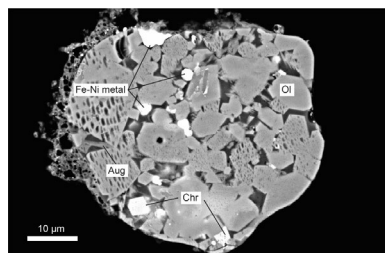


Fig. 1. BSE image of the TP T227.8.F1, FeO-rich chondrule fragment. Ol = olivine; Aug = augite; Chr = chromite.

The TP, T227.8.F1, is a chondrule fragment composed of FeO-rich olivine, Fe-Ni metal, chromite,

augite, and albitic glassy mesostasis (Fig. 1). Distinct from typical FeO-rich chondrules in primitive chondrites, it shows uniform olivine compositions (Fo_{62}) without chemical zoning or relict forsteritic cores. However, an isotopically distinct olivine domain with ^{16}O -rich ($\delta^{18}\text{O} \sim -13\text{‰}$; $\Delta^{17}\text{O} \sim -7\text{‰}$) signatures was identified, while the other (11 olivine, 1 augite) analyses display small variations ($\delta^{18}\text{O} \sim 0\text{‰}$ to $\sim 5\text{‰}$; $\Delta^{17}\text{O} \sim -1.5\text{‰}$ to $\sim 0.2\text{‰}$) along the PCM line (Fig. 2).

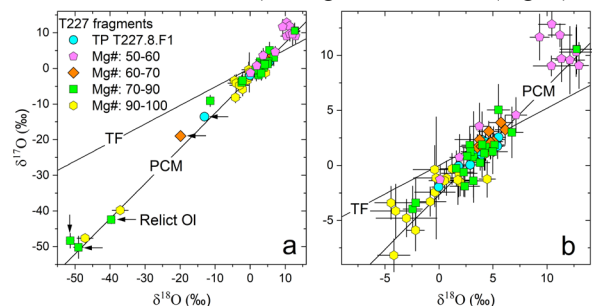


Fig. 2. Oxygen isotope ratios of T227 fragments grouped based on their Mg#.

Mg# = 50-60 (N=7): olivine fragments with Mg# of 52-55. Three contain glassy mesostasis (chondrule-like), two have chromite inclusions, and two are monomineralic. They show variable and significant ^{16}O -poor signatures with $\delta^{18}\text{O}$ and $\Delta^{17}\text{O}$ ranging from $\sim 0\text{‰}$ to $\sim 13\text{‰}$ and from $\sim -1\text{‰}$ to $\sim 7\text{‰}$, respectively. Six analyses on T227.5.1.F3 ($\sim 13 \mu\text{m}$, Fo_{53-54}) display heterogeneous oxygen isotope ratios that almost span this entire range.

Mg# = 60-70 (N=8, exclude TP): olivine fragments with Mg# of 67-69. Four have TP-like igneous texture, three have inclusions of glassy mesostasis, chromite, and/or sulfide, and two are monomineralic. Their oxygen isotope ratios are tightly clustered ($\Delta^{17}\text{O} = 0.6 \pm 1.1\text{‰}$) within the TP range. An exception is one analysis in a chondrule fragment (T227.8.F6) with $\Delta^{17}\text{O}$ decreased from 2‰ to -20‰ within an analysis (shown as mean in Fig. 2), likely to be a relict domain.

Mg# = 70-90 (N=19): thirteen olivine (Ol, Fo_{72-86}) and six low-Ca pyroxene (Lpx, $\text{En}_{75-85}\text{Wo}_{0-9}$) fragments. Four are chondrule-like fragments, i.e., T227.7.2.F11 (Lpx + Ol + glass), T227.4.F4 (Lpx + sulfide + chromite), T227.7.1.F3 (Ol + merrillite + chromite), and T227.5.3.F5 (Kool grain). The other fragments are mono-/polymineralic. T227.4.F24 is a ^{16}O -poor olivine fragment (Fo_{75}) that overlaps with Mg# = 52-55 fragments. Furthermore, one of the two analyses on an olivine fragment (T227.8.F4) and two

analyses on an olivine fragment (Fo₈₄, T227.5.3.F4) with a forsteritic core show significant ¹⁶O-rich signatures ($\Delta^{17}\text{O} \sim -22\%$, Fig. 2), implying a relict origin. The other fragments show $\delta^{18}\text{O}$ and $\Delta^{17}\text{O}$ from $\sim -11\%$ to $\sim 7\%$ and $\sim -3\%$ to $\sim 2\%$, respectively.

Mg# = 90-100 (N=18): eleven olivine, six low-Ca pyroxene (En₇₂₋₉₉Wo₀₋₉), and one Al-diopside (31 wt% Al₂O₃, 0.3 wt% TiO₂, stoichiometry like CaAlAlSiO₆ in CAIs, encloses a PGE metal) fragment. The chondrule-like fragment, T227.5.2.F1, is composed of olivine, low-Ca pyroxene, roedderite, and pyrrhotite. T227.4.F11 is a pure forsterite grain with $\Delta^{17}\text{O} \sim -22\%$. The remaining fragments are ¹⁶O-poor with $\Delta^{17}\text{O}$ ranging from $\sim -6\%$ to $\sim -1\%$, including the CAI mineral-like Al-diopside fragment ($\Delta^{17}\text{O} \sim -1\%$). Their $\Delta^{17}\text{O}$ values, including Mg# > 97 ones, are not correlated with Mg# (Fig. 3b).

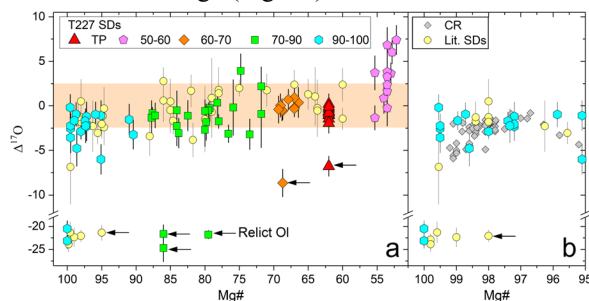


Fig. 3. Mg# vs. $\Delta^{17}\text{O}$ relationship in T227 fragments. Literature Stardust (Lit. SDs) from other tracks [4-9], and CR chondrules [11] are plotted for comparison.

Discussions: The seven Mg# = 52-55 olivine fragments, occasionally with mesostasis/chromite inclusions, show similar chemistry but variable oxygen isotope ratios, suggesting they were derived from a large chondrule represented by T227.5.1.F3. They show significant ¹⁶O-poor signatures that haven't been reported in other Wild 2 tracks [4-9]. Similar oxygen isotope ratios have only been found in CH-CB iron-poor chondrules but not iron-rich ones [13]. The eight Mg# = 67-69 olivine fragments, with three have TP-like texture, show indistinguishable oxygen isotope ratios that are within the range of TP. Thus, they were segregated from another large TP-like chondrule.

The oxygen isotope ratios of T227 Mg# = 60-100 fragments are within the range of Wild 2 fragments in other tracks [4-9] and overlap mostly with CR chondrules [12]. However, the abundance of FeO-rich (Mg# < 90) fragments in T227 ($\sim 70\%$) and all Wild 2 tracks studied ($\sim 60\%$) are significantly higher than FeO-rich chondrules in CR ($\sim 4\%$) and most other chondrite groups (except ordinary chondrites, [2, 12]). The FeO-rich chondrule-like fragments (T227.8.F1, Torajiro in [4], Iris in [8], etc.) in Wild 2 are typically free of chemical zoning, which are uncommon for

FeO-rich chondrules in CR and other chondrite groups [12]. Furthermore, four relict olivines with $\Delta^{17}\text{O}$ down to -22% are found in T227 fragments (4 out of 39, like Gozen-sama [4]), while they are rare in CR chondrules [11]. In addition, Mg# > 99 fragments with $\Delta^{17}\text{O} \sim -2\%$ are rare in chondrules of CR and other chondrite groups. Thus, Wild 2 chondrule-like fragments are comparable to rare components in CR and possibly other chondrite groups instead of the main population, which could not be explained by random sampling and may indicate the existence of a yet unknown source.

Wild 2 silicate fragments show a wide range of Mg# (100-52) with $\Delta^{17}\text{O}$ values mostly between $\sim -2\%$ and $\sim 2\%$, suggesting that they formed in a very oxidized environment. Minor iron-poor fragments have $\Delta^{17}\text{O}$ down to -6% , and iron-rich ones tend to have higher $\Delta^{17}\text{O}$ (up to 7%), displaying an overall negative correlation with their Mg#, possibly due to the addition or involvement of ¹⁶O-poor ice during their formation, just like CR chondrules [11]. Thus, we speculate that the Wild 2 fragments, especially chondrule-like ones, could have formed late (>3 Ma after CAI [8, 10]) in a localized region farther out than the CR chondrule-forming region and then migrated a short distance to the comet accretion region. If so, impact jetting between planetesimals in the icy outer solar system could be considered a cometary chondrule formation mechanism [14]. The relict olivines with $\Delta^{17}\text{O}$ down to -22% in Wild 2 chondrule-like fragments suggest the existence of AOA-like olivines in their formation region, which were outward transported from the inner disk at the early stage of the solar system [1]. This could be the same for CAIs (Inti) and ¹⁶O-rich olivine and pyroxene fragments in Wild 2 [1, 5-6].

Conclusion: T227 contains abundant chondrule-like fragments that show different characteristics from typical chondrules in most primitive chondrites, which may indicate a chondrule formation event near the comet accretion region in the icy outer solar system.

References: [1] Brownlee, D. E., et al. (2006) *Science*, 314, 1711-1716. [2] Frank, D. R., et al. (2014) *GCA*, 142, 240-259. [3] Brownlee, D. E. (2017) *MAPS*, 52, 471-478. [4] Nakamura, T., et al. (2008) *Science*, 321, 1664-1667. [5] Nakashima, D., et al. (2012) *EPSL*, 357-358, 355-365. [6] Defouilloy, C., et al. (2017) *EPSL*, 465, 145-154. [7] Zhang, M., et al. (2022) *LPS LIII*, Abstract #1057. [8] Oglione, R. C., et al. (2012) *APJ*, 745, L19. [9] Oglione, R. C., et al. (2015) *GCA*, 166, 74-91. [10] Nakashima, D., et al. (2015) *EPSL*, 410, 54-61. [11] Tenner, T., et al. (2015) *GCA*, 148, 228-250. [12] Schrader, D. L., et al. (2015) *MAPS*, 50, 15-50. [13] Krot, A. N., et al. (2010) *GCA*, 74, 2190-2211. [14] Cashion, M., et al. (2022) *Icarus*, 384, 115110.